Applied Thermal Engineering 149 (2019) 788–797

Contents lists available at ScienceDirect

Applied Thermal Engineering

journal homepage: www.elsevier.com/locate/apthermeng

Research Paper

Thermal conductivity of water Ih-ice measured with transient hot-wires of different lengths

Catalina Vélez, Brian Reding, José M. Ortiz de Zárate, Mohamed Khayet*

Department of Structure of Matter, Thermal Physics and Electronics, Faculty of Physics, University Complutense of Madrid, Avda. Complutense s/, 28040 Madrid, Spain

HIGHLIGHTS

- Dependence of the transient hot-wire (THW) signal on the wire length is discussed.
- THW measurements can be performed with wires as short as 4 cm for 50 μm diameter.
- The same THW setup can be used to measure both liquids and solids.
- New experimental values of the thermal conductivity of Ih-ice are presented.

ABSTRACT

Presented in this paper is an investigation on wire-length dependence of transient hot-wire calorimetry, a technique generally used to measure the thermal conductivity of materials. In particular, a measurement protocol that includes the use of a calibration fluid that was designed for wires of reduced lengths; so as to reliably apply the transient hot-wire method to materials exhibiting a solid-liquid phase transition as a function of temperature. An experimental study of the onset of convection was also carried out, including a comparison between measurements performed in the liquid and solid phases. For the purpose of validation, presented are experimental measurements of the thermal conductivity of water Ih-ice at 0.1 MPa, within a temperature range of 259–266 K, and that of n-eicosane within the range of 259–348 K, which encompasses its melting point.

1. Introduction

The transient hot-wire (THW) method is becoming the technique of choice for the accurate measurement of the thermal conductivity $\lambda(T)$ of fluid systems [1] as a function of temperature. Recently, [2,3] this technique was extended to the measurement of $\lambda(T)$ in solid state for systems exhibiting a solid-liquid phase transition at nearly room temperature, so that solidification of the sample takes place inside the measurement cell. Linear alkanes containing between 15 and 20 carbons atoms, commonly used in the formulation of Phase Change Materials (PCM) [2–4], were tested. A good characterization of the thermophysical properties of PCMs is required for their rational use in thermal energy storage and energy efficient systems; as well as in other increasingly important energy applications [4–11]. Specifically, the introduction of PCMs for thermal energy storage has been found [4] to provide solutions in the following areas:

- To bridge the time delay between production or availability of energy and its consumption in receiving systems (solar energy, cogeneration, etc.)
- To improve the security of energy supply (hospitals, computer centres, etc.)
- Thermal inertia and thermal protection

With these materials there are relatively large volume changes occurring during the solid-liquid phase transition [2,3]; this required the addition of more sample material inside the THW measurement cell as crystallization happens. In the present paper, an alternative approach is presented using wires of reduced lengths L; whereas wires of approximately 20 cm were typically used in our previous studies [2,3,12,13]. Additionally, one of the advantages of this approach is the reduction of the sample volume; which simplifies the temperature control system and permits studies with rare and expensive materials.

Other authors have previously used for THW wires with lengths shorter than 20 cm, for instance Assael et al. [14] used two Tantalum wires of 14.5 cm and 5 cm length, Perkins et al. [15] used two Platinum wires of 19 cm and 5 cm length, or Alvarado et al. [16] a single Platinum wire of 12 cm length. In all these cases, results were analysed with the infinite line source model of Eq. (1) mentioned below; while in the first papers [14,15] two wires of different lengths were adopted

* Corresponding author.
E-mail address: khayetm@fis.ucm.es (M. Khayet).

https://doi.org/10.1016/j.applthermaleng.2018.12.073
Received 13 June 2018; Received in revised form 1 December 2018; Accepted 12 December 2018
Available online 13 December 2018
1359-4311/

Nomenclature

List of symbols

Symbol	Meaning (Units (SI))
A	wire calibration constant, see Eq. (7) ($\Omega\ m^{-1}\ K^{-1}$)
a_T	thermal diffusivity ($m^2\ s^{-1}$)
$\left(\frac{dT}{d\ln t}\right)$	temperature logarithmic slope (THW signal) (K)
$\left(\frac{dV}{d\ln t}\right)$	voltage logarithmic slope (THW signal) (V)
Fo	Fourier number, $Fo = a_T t/r_0^2$ (Dimensionless)
I	electrical current (A)
L	wire length (m)
m	slope of $R(T)$ dependence, see Eq. (3) ($\Omega\ K^{-1}$)
N	systematic error (deviation) when evaluating λ by Eq. (2) (Dimensionless)
$\dot{q}$	heat dissipated in the wire per unit length ($W\ m^{-1}$)
R	electrical resistance (Ω)
r_0	wire radius (m)
S	wire cross section (m^2)
T	wire temperature (K)
ΔT	temperature difference (K)
t	time (s)
V	voltage drop along the wire (V)
α	temperature coefficient of resistance for wire material (K^{-1})
γ	Euler's constant, $\gamma \simeq 0.577$ (Dimensionless)
λ	thermal conductivity ($W\ m^{-1}\ K^{-1}$)
ρ	electrical resistivity (Ω m)

Subscript

0	initial values, at $t = 0$
max	maximum value during a wire heating

trying to eliminate axial heat conduction. For the current investigation a different approach was considered, and the theoretical work by Blackwell [17,18] was applied to assess the THW signal dependence on wire length, which allows the use of THW with single wires of length down to 4 cm. In addition, further details about the protocol developed for the $\lambda(T)$ measurement of PCMs [2,3] will be presented in this paper. Specifically, this protocol requires a preliminary study of convection in the liquid state as well as a calibration of the short wires with a material of known $\lambda(T)$. To validate the proposed protocol, experimental values of the thermal conductivity of H_2O Ih-ice at 0.1 MPa and at temperatures down to 258 K are used. Confirmation of the reliability of using short wires is accomplished by measuring n-eicosane in both solid and liquid phases (i.e. within the temperature range of 258–340 K encompassing the melting point). Having a melting point close to room temperature, n-eicosane is increasingly used in the formulation of PCMs [4] and the current results may be relevant for the energy storage and conservation community.

The material in this paper is presented as follows: In Section 2 the experimental setup and the THW method is briefly discussed. Followed by, in Section 3, a review of various theoretical studies on how the THW method signal depends on the length of the hot wire and additionally describing in more detail the modifications adopted in the experimental setup of the THW protocol to use wires of reduced lengths; which allows for one to readily measure in both solid and liquid states. An important issue in the broadening of the THW method to short lengths wires is the selection of the Fourier number (Fo), that is correlated to the onset of convection in liquid samples, which is specifically discussed in Section 4. Finally, in Section 5, some experimental results obtained with wires of reduced lengths are presented, including: calibration with water and the associated issue of selection of the amperage range. Thermal conductivity values for water *Ih*-ice (down to the temperature of 258 K), along with the $\lambda(T)$ values of n-eicosane are presented for the temperature range 257–340 K, which encompasses its melting point.

2. Experimental technique and setup

If at time $t = 0$ an electrical current of constant amperage I starts to circulate through a conducting wire kept initially at T_0, because of Joule heating, the wire temperature $T(t)$ increases with time. The rate of temperature increase depends on the heat transferred to the medium that surrounds the wire. When the heat transfer is by heat conduction only, the temperature $T(t)$ can be evaluated by solving the time-dependent heat equation [19,20]. The most straightforward approach is to model the wire as a linear uniform heat source, and adopt a Green (or source) function in cylindrical coordinates (i.e. equivalent to assume the wire is of zero radius and infinite length), in which case an analytic solution can be readily obtained [12,19]. Asymptotically for large t, the solution simplifies to [12,19]:

$$\Delta T = T(t) - T_0 = \frac{\dot{q}}{4\pi\lambda}\left[\ln\left(\frac{4a_T}{r_0^2}t\right) - \gamma\right] \tag{1}$$

where $\dot{q}$ ($W\ m^{-1}$) is the heat dissipated in the wire per unit length, so that in the case of Joule heating $\dot{q} = I^2 R_0/L$, with R_0 being the electrical resistance of the wire and L its length. Other quantities in Eq. (1) are the thermal diffusivity a_T and thermal conductivity λ of the continuum medium surrounding the wire, the radius r_0 of the wire (assumed cylindrical) and the Euler constant $\gamma = 0.5772$. Eq. (1) is an asymptotic expansion for long times of the analytical full solution; hence, it will be only valid for heating runs of duration $Fo >> 1$ (in terms of the dimensionless Fourier number, $Fo = a_T t/r_0^2$). For the determination of the thermal conductivity, Eq. (1) is rewritten as:

$$\lambda = \frac{\dot{q}}{4\pi}\Big/\left(\frac{dT}{d\ln t}\right) \tag{2}$$

where $(dT/d\ln t)$ indicates the logarithmic slope of the heating curve, named hereafter as the THW signal. In the implementation of the THW method what is actually measured is the voltage difference $V(t)$ between the wire ends as a function of time. The wire temperature $T(t)$ is related to $V(t)$ by Ohm's law and if one assumes for an electrical

Table 1
Intercept R_{273} and slope m obtained from fitting to Eq. (3) the data in Fig. 4 adopting $T_0 = 273$ K as reference temperature. Corresponding values for: α_{273}, L_{eff}, see Eq. (8), calibration constants, see Eq. (6), and L_{app}, see Eq. (9), are also tabulated.

	L (cm)	$R_{273}(\Omega)$	m (Ω/K)	α_{273} (K^{-1})	L_{eff} (cm)	A ($\Omega K^{-1} m^{-1}$)	L_{ap}(cm)
Wire 1	11.5	5.621	0.02198	3.910×10^{-3}	11.38	0.01521	11.5
Wire 2	6.5	3.181	0.01255	3.945×10^{-3}	6.44	0.01664	6.0
Wire 3	4.0	1.968	0.00763	3.877×10^{-3}	3.98	0.01518	4.0

conductor a linear dependence

$$R = R_0 + m(T - T_0) \tag{3}$$

of its electrical resistance on temperature. The slope m in Eq. (3) is proportional to the temperature coefficient α of the electrical resistivity of the wire material ($m = \alpha R_0$).

The implementation of the THW method in the laboratory and the corresponding experimental setup has been extensively described in previous publications, where it was successfully applied to measure $\lambda(T)$ at atmospheric pressure of pure liquids [12], nanofluids [13,21], clays [22] and PCMs (hydrocarbons or paraffins) [2,3]. Hence, only a brief summary emphasizing the modifications adopted for the use of short wires are presented here. The core of the apparatus is a platinum wire, with a diameter of 50 µm. In the present study three different wires with different lengths, namely W1 (L = 11.5 cm), W2 (L = 6.5 cm) and W3 (L = 4 cm), were employed as further described below in Table 1. Each wire was mounted in a specifically made custom plastic frame to keep it straight. Fig. 1 left panel shows a photograph of one of the wires mounted in its frame. At each end of the platinum wire two electrical connecting cables are soldered and the connections are covered with an insulating epoxy resin.

Then, the frame together with the wire was placed vertically inside a double walled glass cell filled with the test sample at a temperature for which the specimen is in a liquid state. The temperature of the measurement cell is controlled by using a thermostatic circulator (Lauda ECO RE630) and a controlled environmental chamber. The external probe of the thermostatic circulator was inserted into the measurement cell, thus allowing for a wide range of specimen temperature measurement and control. Measurements of the specimen while in solid state were performed by reducing the specimen temperature, so that solidification occurred *in-situ* (in the same cell). Since the liquid-solid phase transition induced important volume changes, in this study, shorter wires than those considered in previous investigations were implemented [2,3,12,13,21,22]. By adopting this modification, the wire with its supporting frame only occupied the bottom of the measurement cell, leaving sufficient space above the wire to safely compensate for any change in volume of the sample during the phase change.

Once the temperature of the sample is stabilized at T_0, with the sample either in its solid or liquid state, individual heating trials were performed by administrating a DC electrical current of known intensity (I) through the wire for a short duration; the duration is always less than the time for convection to arise (a more detailed discussion can be found in Section 4). In the implementation of the THW method, for a given T_0, hundreds of individual heating trials were performed using different amperages within a given range; such an approach is referred to as multi-current THW method [12]. In previous publications extensive statistical analysis was conducted [13,22], showing how the use of different amperages enhanced the reliability of the final $\lambda(T)$ values. For the electrical measurements, a computer-controlled Keithley 2400 source meter was employed. The 4-wire sense mode was utilized, thus the electrical resistance and/or voltage drop in the connecting cables is compensated by the measurement apparatus. For the present study, the reference temperature T_0 was obtained from the circulation bath external probe, which was also computer-controlled. The right panel of Fig. 1 shows a schematic of the experimental setup and its various components.

To summarize the experimental procedure: Once the cell has reached the desired initial equilibrium temperature T_0 (with the sample either in the solid or the liquid state) the data acquisition system and experiment controller was initiated. Hundreds of individual heating trials were performed using different amperages within a given range and the data digitally recorded. For each individual heating trial the following is conducted:

- The initial temperature is recorded (acquired from the external

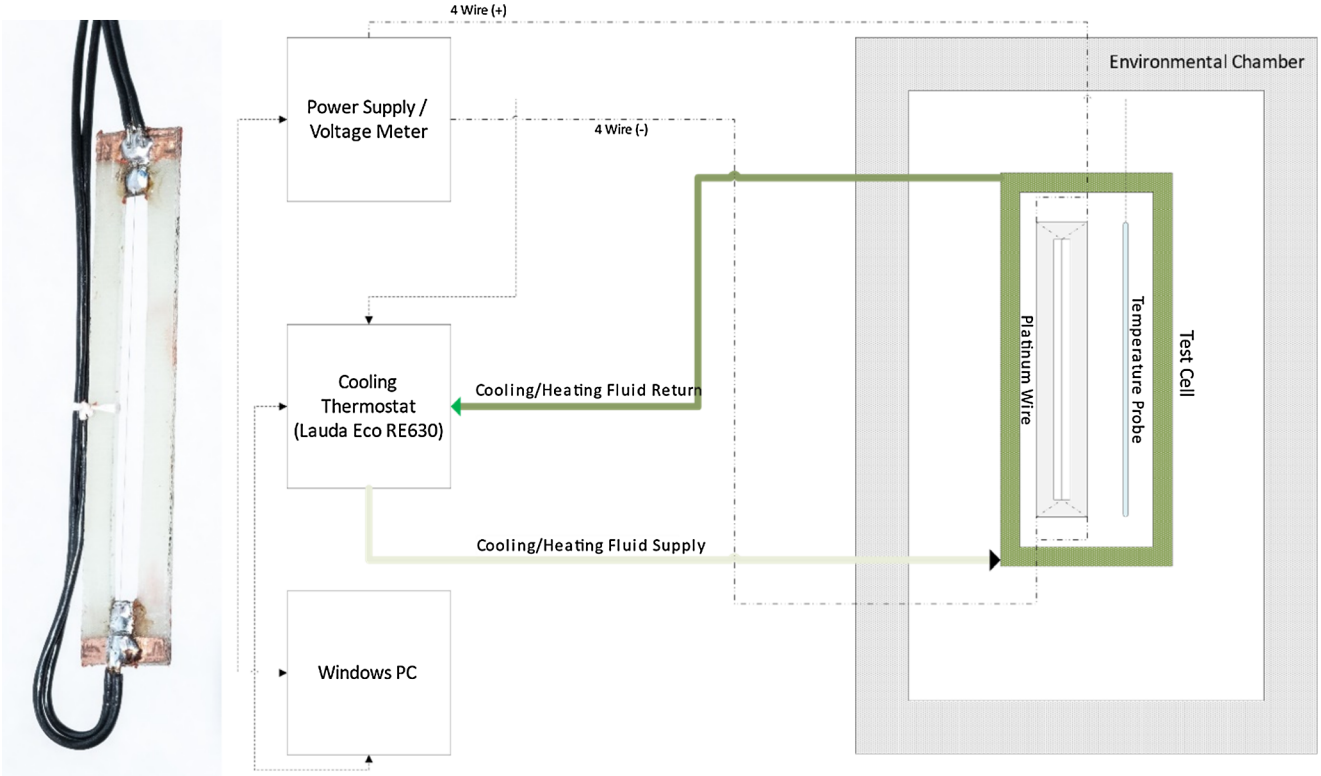

Fig. 1. Left: one of the wires mounted in its plastic frame, with two connectors soldered at each end and before covering the solder with insulated epoxy resin. Right: Schematic representation of the experimental setup (platinum wire and frame inside the measurement cell, thermostatic circulation bath, Keithley 2400 source and meter, desktop computer, digital thermometer for chamber control, Temperature controlled chamber).

probe of the thermal bath)
- The initial electrical resistance (measured by the Keithley 2400 source-meter),
- After a delay time of one second, the electrical source is turned on and voltage is measured as a function of time
- Once the heating trial is ended the computer reads the voltage measurements and evaluates the logarithmic slope, $(dV/d\ln t)$, by fitting the registered $V(t)$ data points acquired after at least 100 ms of heating (because of the $Fo >> 1$ condition) and before convection sets in.

A 5 min waiting time was established between two consecutive heating trials, to let the system return back to its equilibrium state. Once a series of individual heating trials was completed, the initial equilibrium temperature T_0 was changed manually, and the whole process repeated.

3. Dependence of the THW signal on the finite length of the wire and experimental protocol for short wires

Eqs. (1) and (2) were obtained under the assumption of a wire of infinite length. Many studies have been devoted to systematic errors in the THW method associated to finite radius and length of the hot wire [17,18,23]. In particular, by Blackwell [17,18], Healy et al. [23] and Liang [24] in the past century, and more recently by Elustondo et al. [25]. In this section we briefly review these theoretical studies and how they justify the approach followed to perform the measurements with short-wires.

The original work of Blackwell [17,18] characterized finite-length effects by introducing a systematic error N when Eq. (2) is used to evaluate $\lambda(T)$. Namely, because of the wire finite length, instead of Eq. (2) one would have:

$$\lambda = (1 - N)\left[\frac{\dot{q}}{4\pi}/\left(\frac{dT}{d\ln t}\right)\right] \tag{4}$$

Blackwell [17,18] solved the time-dependent heat equation in cylindrical coordinates for the region $r_0 < r < \infty$. To model the finite length of the wire in the axial z-direction, the boundary conditions at $r = r_0$ changed from a constant (radial) heat flow for $|z| < L/2$, to zero heat flow for $|z| > L/2$. Hence, the wire is itself infinite, but only the $|z| < L/2$ is in contact with the surrounding medium and transfers heat to it, while the rest is insulated. With these assumptions, Blackwell [17,18] was able to obtain an analytic expression for the dependence of the error N on time and wire length, namely:

$$N = 1 - \mathrm{erf}\left(\frac{L}{4\sqrt{a_T t}}\right) = 1 - \mathrm{erf}\left(\frac{\eta}{2\sqrt{Fo}}\right) \tag{5}$$

where in the second part of Eq. (5), the wire aspect ratio $\eta = L/2r_0$ and the Fourier number are used. Equation (5) implies that for smaller aspect ratios (shorter wires) the error N becomes larger, and only when $\eta \to \infty$ the error is zero, and Eq. (2) applies exactly. Since the error N also depends on time, because of finite L, one initially does not expect a constant logarithmic slope during a heating run. However, according to Eq. (5), N is a monotonically increasing function of time, so that the maximum error attained becomes bounded by the duration of the experiment. In what follows, to make sure that systematic errors associated to finite L do not exceed a certain limit, time in Eq. (5) shall be substituted by the maximum time. In conclusion, for larger Fo numbers, the error also becomes larger.

Later works by Healy et al. [23], Liang [24], and Elustondo et al. [25] depend on the original results of Blackwell, summarized here by Eqs. (4)–(5).

The THW method initially allows for an absolute determination of $\lambda(T)$ [26–28]. However, a completely absolute measurement requires corrections for the various sources of systematic errors. Note that, in general, systematic errors are not only associated to the finite dimensions of the wire, but to other contributions as well; for instance, wire self-heating, synchronization of the measurement devices, time spent in current ramping, possible electrical conduction to the surrounding medium, etc. Hence, true absolute measurements tend to be quite demanding. For these reasons, in some publications [13], is proposed an alternative, simpler, calibration approach that gives only $\lambda(T)$ values relative to a calibration fluid. This approach [13] consists in reworking the combination of Eqs. (2), (3) and Ohm's law as:

$$\lambda = AI^3R_0/\left(\frac{\mathrm{d}V}{\mathrm{d}\ln t}\right) \tag{6}$$

where A (SI units $\Omega\,\mathrm{K}^{-1}\mathrm{m}^{-1}$) is to be interpreted as a "calibration" constant that depends on the wire characteristics, but it is independent of the sample under test, and the temperature or the amperage I. Then, a calibration fluid whose thermal conductivity is known can be used to infer the value for A of a given wire. If measurements with a calibration fluid are performed at various temperatures, a better estimation of A can be derived [13]. Once this value is correctly determined for a given wire, the unknown thermal conductivity of other materials can be measured using the same Eq. (6) and the acquired values of amperage, electrical resistance and logarithmic slope $(dV/d\ln t)$.

Notice that the wire finite length effects, according to Blackwell theory [17,18], can be considered as consistent with the calibration approach. Indeed, if wire finite dimensions were the only source of systematic errors, a theoretical value for the calibration parameter A can be obtained by combining Eqs. (3) and (4) with Joule dissipation $(\dot{q} = I^2R_0/L)$ and Ohm's law, namely:

$$A = \frac{m}{4\pi L}\left[1 - N(L)\right] = \frac{\alpha\rho}{4\pi S}\left[1 - N(L)\right] \tag{7}$$

where ρ is the electrical resistivity of the wire material and $S = \pi r_0^2$ the wire cross section. Eq. (7) means that the effects of the wire finite length, embodied into the parameter N (whose dependence on L has been here explicitly indicated) can indeed be incorporated into the wire calibration constant A. Hence, we conclude that the indirect wire-calibration approach, which was already used with long wires [13], can be extended to short wires and will safely account for finite-length effects. In this case the wire parameter A will depend on L and on the duration of the experiment (Fo number), see Eq. (5).

We finalize this section by remarking that the relative measurement technique we adopt here, like any calibration method, is expected to work better when the calibration and the test samples do not differ much in the values of the measured quantity. As further discussed in Section 5, for the present paper, the difference in λ between the calibration fluid and the tested samples is not larger than one order of magnitude and the obtained results appear to be reliable.

4. *Fo* selection and convection

An important parameter in the THW experiments is the duration of the wire heating, which is conveniently represented by the dimensionless Fo number. Concerning Fo selection, Eqs. (2) and (5) imply contradictory requirements. Indeed, Eq. (2), and its resulting Eqs. (4) and (6), require $Fo >> 1$, while Eq. (5) indicates that the systematic error associated to finite length of the wire increases for larger Fo. In addition, there is another important consideration concerning Fo selection. The presence of gravity (buoyancy) causes the THW method configuration to be intrinsically unstable for fluids, so that, unavoidably, convection will appear [29–32]. This fact does not completely spoil the use of THW method with fluids, because due to viscous effects convection does not appear immediately after initiating an amperage I, and there is a time delay, t_D, before convection is established. For $t < t_D$ the fluid can be considered quiescent and the THW method equations of the previous section continue to be valid.

With a combination of computational fluid dynamics (CFD) and

experimental studies it can be concluded [29–32] that the appearance of convection in the THW method depends primarily on the *Fo* number. Typically, convection develops for *Fo* numbers between 500 and 1000, depending weakly on the heating rate and the fluid viscosity. Thus, Zhang & Fujii [31] proposed as a rule for the THW method to be free of convection to keep *Fo* numbers below 200–300; which for the samples and wire radius used in this paper, are interpolated to about 1.6 s. It should be noted that the extensive work of Rusconi et al. [32] with water and ethylene glycol showed that 1.6 s was always below their experimental or computational delay times t_D.

To check the proper selection of *Fo* numbers, a preliminary experimental study on convection was performed employing the wire W1. As an illustration, Fig. 2 shows three heating curves (wire temperature increase as a function of time) obtained with W1 in n-eicosane. Two curves are at $T_0 = 318$ K (i.e. with n-eicosane in liquid state) and one curve is at $T_0 = 268$ K (i.e. with n-eicosane in solid state). For simplicity, the W1 electrical properties in Table 1 have been used here to represent the actual wire temperature instead of the directly measured voltage drop. Fig. 2 shows that, as expected, convection indeed appears after 3–5 s. As extensively described by Rusconi et al. [32], the indication of the onset of convection is a significant deviation from the constant logarithmic slope at times larger than t_D, which is clearly observed in the two heating curves of Fig. 2 in liquid state. Notice that when n-eicosane is in solid state and convection is impossible, those deviations do not exist. By comparing the two curves in liquid state in Fig. 2 it is also confirmed that the appearance of convection depends mainly on *Fo* and only weakly on the heating rate [31].

In addition to the large time deviations due to convection, Fig. 2 also shows some short time deviations from the constant logarithmic slope. In this regard it is reminded that Eq. (1) is only an approximation valid for large times; which in practice, for the wire radius used and the typical thermal diffusivity of tested samples, signifies a heating trial duration longer than approximately 100 ms [12]. It is very likely that systematic errors other than the approximations in the theory are contributing to these short time deviations, including source synchronization or the finite time needed to initiate the amperage.

Nonetheless, regarding *Fo* selection, it is clear from Fig. 2 that even for fluid samples, there exists a sizable *Fo* range for which the logarithmic slope of the THW method signal can be considered as uniform. To illustrate this, the data points in Fig. 2 acquired in the range from 0.25 s to 1.43 s, with the sample in liquid state (represented as a shadowed region), have been fitted to a constant logarithmic slope function of time, $\Delta T = a + b \ln t$, with the results being represented as red lines. It is evident in Fig. 2, that experimental data points in this range are indeed well represented by a constant logarithmic slope and meaningful and reproducible values for $(dT/d\ln t)$ can be obtained. This time range, roughly corresponding to $10 < Fo < 100$, is good enough to fulfill the $Fo \gg 1$ condition and, simultaneously, the $Fo \leq 200$ condition to avoid the onset of convection [31]. Furthermore, systematic errors associated to wire finite length are not expected to be too large in this *Fo* range, see Eq. (5).

In addition to a careful *Fo* range selection, a sensible application of the THW method also requires a detailed discussion of amperage range, which will be presented in Section 5.1 in association with the wire calibration procedure.

5. Experimental results

The material presented in this section is split into three different subsections. First, in Section 5.1, the calibration of short wires is considered, which includes a discussion of the range in amperage and the measurement of water. Then, in Section 5.2, validation for the use of short wires is presented, by reporting values of the thermal conductivity of water Ih-ice. Finally, in Section 5.3, further validation studies are discussed, including $\lambda(T)$ values for n-eicosane in both liquid and solid states, which compare favorably with previous measurements using longer wires [2].

5.1. Calibration of short wires

As has already been stated, in the present study we have used three different wires (W1, W2 and W3) of different lengths as specified in Table 1. As elucidated in Section 3, the approach requires the calibration of the short wires with a sample of known $\lambda(T)$. Water was chosen as the calibration fluid because standard reference data and recommended correlations as a function of temperature are readily available [27]. The water used for these experiments has been double-distilled in the laboratory.

To obtain a better estimation of the calibration constant *A*, heating trials with water at different temperatures in the range of 278–328 K were performed. For each wire and each temperature, several hundred individual heating trials, as those shown in Figs. 2, 3 were recorded. Consistent with the discussion of Section 4, and depending on the wire used, the duration of these individual runs was always set to less than 1.4 s, while various values for the amperage were applied. The main consideration for the amperage value selection is to have good signal to noise ratios; the higher the amperage the greater the voltage drop along the wire (signal). This requirement is particularly important for short wires; as electrical resistance becomes smaller. Hence, higher amperages are initially preferred for shorter wires. However, the amperage should not be too large, since a large ΔT induced in the wire and the adjacent medium affects the accuracy of the measured $\lambda(T)$. In this regard, a limit is established for the maximum allowed wire temperature increase as $\Delta T_{max} \approx 7$ K.

Taking into account all previous considerations, a maximum duration of 1.0 s is selected for the longer wire W1, that is well below the convection threshold determined in Section 4. In practice, the data acquisition device (Keithley-2400) is programmed to measure 350 data points at a 'medium' acquisition frequency of about ~300 Hz. To evaluate the experimental logarithmic slope, for wire W1, an interval between 0.5 s and 1.0 s was used; which is well above the $Fo >> 1$ condition. The amperage range for W1 was established at 160–240 mA. Notice that in Fig. 2 it verifies the requirement of $\Delta T_{max} \leqslant 7$K ($\Delta T$ is smaller for water than for n-eicosane and trials stop at 1 s). To acquire better signal to noise ratios for the two shorter wires (W2 and W3), an

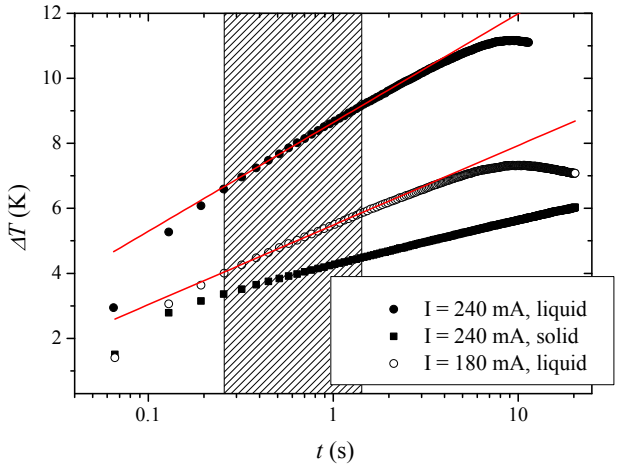

Fig. 2. Temperature increment, ΔT, as a function of time for W1 in n-eicosane at $T_0 = 318$ K (liquid state, round symbols) and $T_0 = 268$ K (solid state, square symbols). Filled symbols are for an amperage of $I = 240$ mA and open symbols for $I = 180$ mA. Red lines represent fittings to $\Delta T = a + b \ln t$ of the experimental data points measured between t = 0.25 s and t = 1.43 s (shadowed range). Observe how, only when the sample is in liquid state, convection appears at about 3–5 s, depending only weakly on the applied electric current [32]. (For interpretation of the references to colour in this figure legend, the reader is referred to the web version of this article.)

increase in the amperage range to 350–390 mA was required. As a consequence, and to keep $\Delta T_{max} \leqslant 7$K, the duration of the trials had to be reduced to 0.4 s. In practice, the data acquisition device (Keithley-2400) was programed to measure 350 data points at a 'fast' acquisition frequency of about ~ 800 Hz. To evaluate the experimental logarithmic slope, for wires W2 and W3, an interval between 0.2 s and 0.4 s was used, which is within the range established in Section 4 in relationship with the *Fo* selection. Lastly, it should be noted that, since ΔT_{max} depends also on the thermal conductivity of the sample under test, for measuring samples in solid state the amperage range had to be adjusted, using slightly larger values in particular for the shorter W3.

To illustrate the amperage range selection Fig. 3 shows a series of individual heating trials (i.e. representation of voltage drop along the wire as a function of time) obtained with water and, thus, representing calibration trials. The two top panels are for the longer wire W1, and include a trial at an initial temperature $T = 288$ K and another trial at an initial temperature $T = 328$ K. The two bottom panels are for wires W2 (bottom left) and W3 (bottom right). Note that, as explained, the duration of the trials is shorter for the wires W2 and W3 (bottom panels). The amperage values, as indicated in Fig. 3, are intermediate in the range selected for each wire. For all the plots in Fig. 3 the final wire heating is about 6 K. Compared to Fig. 2, no signs of convection are observed. Red straight lines in Fig. 3 represent a constant logarithmic slope fitting of the data acquired after 500 ms (for W1) or 200 ms (for W2 and W3). In all cases, the experimental points are well represented. It must be pointed out that the trials with the shorter wires (bottom panels) have a smaller signal to noise ratio in spite of the larger current values.

To calibrate the wires, hundreds of individual heating trials, similar to those shown in Fig. 3 were performed. As indicated previously, the measurement protocol includes, for each individual heating trial, to register the initial electrical resistance and temperature, acquired one second before swithching the amperage source on. From these measurements, the dependence $R(T)$ can be investigated, as it is shown graphically in Fig. 4 for the three wires and all the trials with water. For completeness, trials with wires W1 and W3 performed at lower temperatures, with water in solid state (see Section 5.2) and are also included here. The data points shown in Fig. 4 represent averages over hundreds of individual values, and the corresponding standard deviations (both in R and T) are not larger than the symbol size.

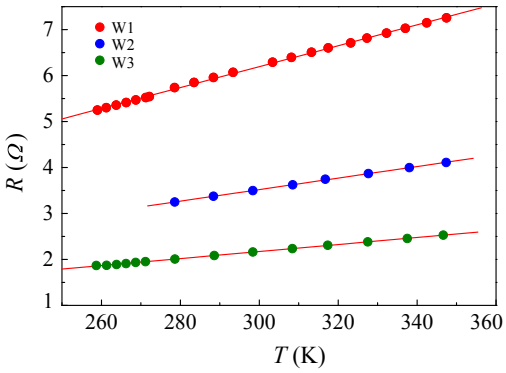

Fig. 4. Electrical resistance as a function of temperature $R(T)$ of the three wires. Includes all the runs performed with water, including liquid and solid state. Linear fitting of the data to Eq. (3) are displayed as red lines. (For interpretation of the references to colour in this figure legend, the reader is referred to the web version of this article.)

The red lines in Fig. 4 show a linear fit of the experimental data as indicated by Eq. (3). In all three cases, the data is in excellent agreement. Using as reference the temperature $T_0 = 273.15$ K, fitted numerical values for the slope m and the intercept R_{273} are summarized in Table 1. The ratio of these two quantities provides the temperature coefficient, $\alpha_{273} = m/R_{273}$, whose values are also reported in Table 1 and agree well with the tabulated reference value for Platinum ($\alpha_{Pt} = 3.90 \times 10^{-3}$ K^{-1}). Furthermore, from the reference value of Platinum electrical resistivity at $T_0 = 273$ K ($\rho_{273} = 9.7 \times 10^{-8}\,\Omega\cdot$m) one can obtain an effective wire length L_{eff}, which we define from Eq. (7) as:

$$R_{273} = \frac{\rho_{273}}{\pi r_0^2} L_{eff} \tag{8}$$

The corresponding effective lengths for each wire are also presented

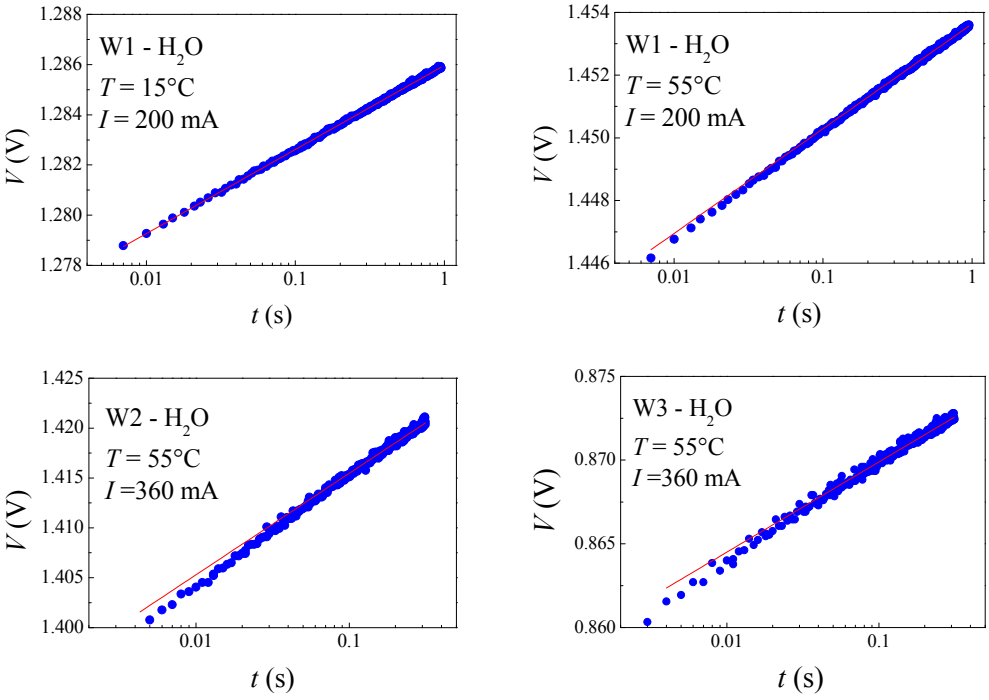

Fig. 3. Examples of experimental heating trials (semi-logarithmic plot of voltage drop along the wire as a function of time) for W1 (top panel), W2 (bottom panel, left) and W3 (bottom panel, right) obtained with water as a calibration liquid. Different initial temperatures and heating amperages, as indicated.

in Table 1. The difference between L_{eff} and the actual length of the wires is in all cases less than 1%. This insignificant deviation is likely related to the systematic errors associated to the actual length measurement, electrical connections, soldering and/or not full compensation of the 4-wire measurement mode of the multimeter.

For each individual heating trial, similar to those shown in Fig. 3, a value for the logarithmic slope is obtained and the ratio $I^3R_0/(dV/d\ln t)$ evaluated. According to Eq. (6), such a ratio is proportional to the thermal conductivity of the sample. The evaluation of the best value for the proportionality coefficient A (calibration constant) is done from the plot shown in Fig. 5, where average values of measured $AI^3R_0/(dV/d\ln t)$, together with their respective standard deviations, are plotted as a function of the initial temperatures T_0, and a background of reference values for $\lambda(T)$ of water [27,33,34]. Then, a value for the calibration constant A is selected so that the measured $AI^3R_0/(dV/d\ln t)$ better agrees with the reference $\lambda(T)$. In Fig. 5 the A value considered optimum for each wire is already used. The numerical A values for the three wires were displayed in Table 1. A simple recollection of Fig. 5 shows that, in all three cases, a single value for the wire calibration constant A represents well the thermal conductivity $\lambda(T)$ of water in the entire temperature range. At higher temperatures a larger dispersion in the measured values is observed. This phenomenon is typical in THW measurements and we have deduced it [12] to be due to the reduction in liquid viscosity.

From the calibration constant A an apparent wire length, L_{app}, can be computed for each wire, by assuming negligible systematic errors N in Eq. (7), namely

$$L_{app} = \frac{m}{4\pi A} \tag{9}$$

The last column of Table 1 depicts the corresponding L_{app} values. It is worth noting that, except for W2, these L_{app} are equal (within 1%) to the actual length L of each wire. In the case of W2 the difference is about 7%, larger than for the other two wires, but still roughly in the range of the few percent intended in this paper. This may be attributed to the fact that this wire was not maintained well straight and tense in the plastic frame during the different cycles of solid/liquid measurements of $\lambda(T)$. We consider that, with the information available, this difference is only marginally significative. A more systematic investigation, using a larger number of wires, will be necessary to settle the significance of this finding.

It is concluded that, in spite of having finite radius and short lengths, the systematic errors associated with the implementation of the THW method are no larger than 7%. In any case, it is of the same order as the reproducibility of the measurements as shown in Fig. 5.

5.2. Thermal conductivity of water Ih-ice

Since only measurements with liquid water were used in the calibration process, the data in solid state obtained with W1 and W3 should actually be considered as independent measurements, from which values for the thermal conductivity of water Ih-ice (the stable form under a standard pressure of 0.1 MPa) could be obtained. It is worth noting that little experimental data obtained by the THW method is available from the literature for the λ of Ih-ice. In Table 2 the numerical $\lambda(T)$ values measured in this investigation are reported; distinguishing between those obtained with W1 and W3.

Thermal conductivity measurements of Ih-ice were not easily obtained. During trials, bubble formation and sub-cooling was observed if water was slowly cooled. Hence, a protocol for a quick flash solidification, programming the thermostatic bath at 258 K, and then waiting overnight before starting the measurements was deemed best practice. Furthermore, important volume changes were observed with water solidification, so that enough compensation volume must be present in the measurement cell. Another complication is that the atmospheric chamber cannot maintain freezing temperatures; which made it very important to have a large volume of ice above the top of the wire for better temperature control. These two last realities are the main reason why Ih-ice measurements could only be performed with shorter wires. In practice, the sample volumes used with water were about 200 cm^3 for W1 and about 50 cm^3 for W3.

The measurements of water Ih-ice $\lambda(T)$ reported in Table 2 are displayed graphically in Fig. 6, and compared with some literature reference values and correlations [34–37]. In the THW theory (see Section 2) it is implicitly assumed that all heating generated in the wire is dissipated through heat conduction to the surrounding medium. But when the sample is in solid state and the initial temperature is not far from the melting point, part of the heat will be dissipated as enthalpy of fusion. Therefore [2,3], the measurements performed with water Ih-ice at initial temperatures inside a $\Delta T \approx 7$ K range below the melting point should be considered incorrect. For completeness, effective conductivities obtained within this range were included in Fig. 6 as open symbols although, due to their lack of reliability, were not reported in Table 2. Some attempts have been made to 'correct' the THW measurements and take into account the enthalpy of fusion effect [19], but the theory available for that is probably too idealistic (homogeneously advancing freezing fronts) and not very useful in practice. For completeness, some higher temperature data points (already shown in Fig. 5) are also added, as obtained with the same wires when the sample is in liquid state.

It can be seen in Fig. 6 that the reproducibility (error bars) for Ih-ice is about 7% for W1 and 10% for W3. These numbers are significantly larger than those for water plotted in Fig. 5. This is not a problem of the THW method when applied to solids, but is most likely related to the lack of homogeneity of the sample itself.

The thermal conductivity of water Ih-ice has been studied by various authors over the years [34–36,38]. A summary of works prior to 1958 was published by Powell [34], while works published after that date and before 1980 were reviewed by Slack [38]. Powell [34], proposed the following linear correlation for the thermal conductivity of water Ih-ice as a function of temperature:

$$10^{-2}\lambda(T) = 0.0209 \times [1 - 0.0017\cdot(T - 273.15)] \tag{10}$$

valid in the range 103–273 K [34] and at a pressure of 0.1 MPa. Ratcliffe [35] also performed experimental measurements of ice by a stationary method and proposed the correlation in the form of a second-order polynomial, namely [35]:

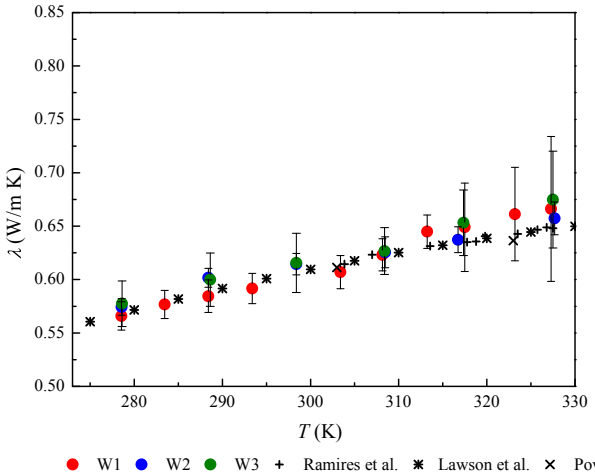

Fig. 5. Calibration with water: For each of the three wires, average values of $\lambda = AI^3R_0/(dV/d\ln t)$, Eq. (6), are represented with their standard deviations, as a function of the (average) initial temperature. The A values are the ones deemed as best for each wire, as reported in Table 1. Reference values for the $\lambda(T)$ of water are those of Ramires et al. [27], Lawson et al. [33], and Powell [34].

Table 2
Thermal conductivity of water Ih-ice at various temperatures as measured with W1 and W3. The reported accuracy represents only random errors (reproducibility). A systematic error estimated to be approximately ± 7% needs to be accounted for.

W1		W3	
T (K)	λ (W/m K)	T (K)	λ (W/m K)
259.01	2.37 ± 0.07	258.73	2.37 ± 0.15
261.25	2.32 ± 0.05	261.33	2.16 ± 0.14
263.76	2.21 ± 0.09	263.83	2.30 ± 0.12
266.29	2.03 ± 0.06	266.23	2.40 ± 0.15

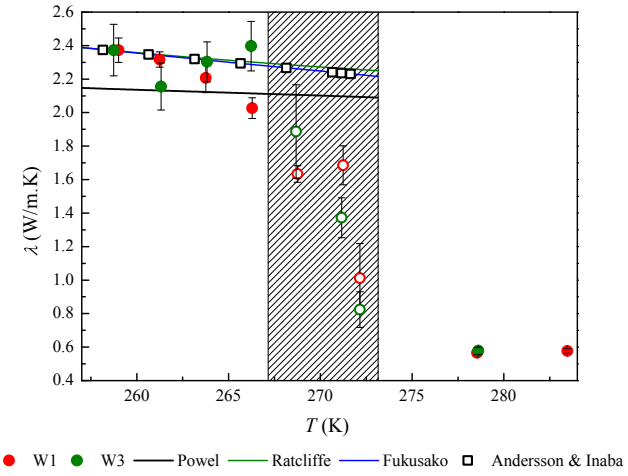

Fig. 6. Thermal conductivity of water Ih-ice as a function of temperature. Filled symbols represent the reliable data (same as in Table 2). Open symbols indicate data affected by enthalpy of fusion (and not reported in Table 2, see text), whose temperature range is indicated as a shadowed region. Some literature measurements and correlations are added for comparison, namely: Powel [34], Ratcliffe [35], Fukusako [36] and Andersson & Inaba [37]. For completeness, some higher temperature data points (already shown in Fig. 5) are also added, as obtained with the same wires when the sample is in liquid state.

$$10^4\lambda(T) = 22500 - 62\,(T - 273.15) + 1.15\,(T - 273.15)^2 \quad (11)$$

for the range 93–273 K and a pressure of 0.1 MPa. More recently, after an extensive literature review, Fukusako [36] proposed yet another quadratic correlation:

$$\lambda(\mathrm{T}) = 1.16 \times [1.91 - 8.66 \times 10^{-3}(T - 273.15) + 2.97 \times 10^{-5}(T - 273.15)^2] \quad (12)$$

In the three Eqs. (10)–(12) T should be substituted in K to obtain $\lambda(T)$ in W/m K. The three correlations above were added to Fig. 6 as colored lines. The noticeable small differences among them [34–36] could be ascribed to the different measurement techniques employed and to the sample preparation [36].

None of the experimental data sets used to establish these correlations [34–36] was carried out by the THW method. However, it can be seen that in Fig. 6, the data considered correct of this study (not affected by the enthalpy of fusion, Table 2) is in fairly good agreement. The differences with the λ data reported by Slack [38] are lower than 4%, while with those of Ratcliffe [35] are between 0.15% and 5.3%. In addition to the correlations above, Fig. 6 depicts the λ values reported by Andersson & Inaba [37].

5.3. Thermal conductivity of n-eicosane measured with short wires

To complete the validation of the THW method with short wires, measurements with *n*-eicosane ($C_{20}H_{42}$, T_m = 308.44 K) were performed in solid and liquid states using the three wires (W1, W2 and W3) previously calibrated with water (see Section 5.1). *n*-eicosane was supplied by Acros (catalog# 204375000, www.acros.com) with a nominal purity of 99% and used as provided without further purification. The thermal conductivity $\lambda(T)$ of *n*-eicosane was measured previously in the laboratory with a wire of length 20 cm [2]. In that publication [2] a detailed discussion on *n*-eicosane's physical properties is found, including a number of issues related to its various crystalline phases and information on other thermophysical properties. In this study, only a brief discussion of the new experimental results will be presented.

Hence, using the calibration constant A determined for each wire (see Table 1) the $\lambda(T)$ of *n*-eicosane was obtained in the range of (initial) temperatures from 257 K to 357 K (including the melting point). As before, data was obtained by performing hundreds of individual heating trials at different amperages, using Eq. (6), averaging them over all the trials performed at the same initial temperature and, finally, evaluating the corresponding standard deviation. The duration of the heating and amperage ranges for each wire were the same values used for the calibration with water as described in Section 5.1.

The results obtained in this series of measurements are reported numerically in Table 3 and depicted graphically in Fig. 7. Added to Fig. 7 are the λ(T) values measured with a longer wire [2] as well as other literature data [39–42]. As was the case with water, the

Table 3
Thermal conductivity of n-eicosane at various temperatures as measured with W1, W2 and W3 as indicated. Only correct data, filled symbols in Fig. 7 not affected by the heat of fusion effect, is presented. Thicker cell lines separate data corresponding to solid state (lower temperatures) and liquid state (higher temperatures). The reported accuracy represents only random errors (reproducibility). A systematic error estimated to be approximately ± 7% needs to be accounted for.

	W1		W2		W3	
	T (K)	λ (W/m K)	T (K)	λ (W/m K)	T (K)	λ (W/m K)
Solid	259.17	0.440 ± 0.012	258.81	0.448 ± 0.010	258.77	0.447 ± 0.015
	264.01	0.433 ± 0.011	263.94	0.438 ± 0.006	264.04	0.432 ± 0.014
	268.85	0.427 ± 0.010	268.89	0.425 ± 0.006	268.77	0.430 ± 0.016
	273.76	0.413 ± 0.010	273.69	0.407 ± 0.005	273.72	0.423 ± 0.019
			278.56	0.387 ± 0.010	278.84	0.411 ± 0.015
	282.53	0.399 ± 0.008	283.88	0.387 ± 0.006	283.82	0.398 ± 0.013
Liquid	313.42	0.151 ± 0.004	313.06	0.151 ± 0.001	313.21	0.148 ± 0.003
	323.18	0.149 ± 0.003	323.18	0.150 ± 0.002	318.34	0.147 ± 0.002
	333.14	0.147 ± 0 0.003	332.96	0.147 ± 0.002	322.95	0.145 ± 0.002
	342.97	0.148 ± 0.005	343.06	0.145 ± 0.002	328.19	0.145 ± 0.003
	347.83	0.148 ± 0.005	347.69	0.144 ± 0.002	332.30	0.145 ± 0.002
					337.83	0.143 ± 0.003
					341.80	0.144 ± 0.002
					347.31	0.143 ± 0.004

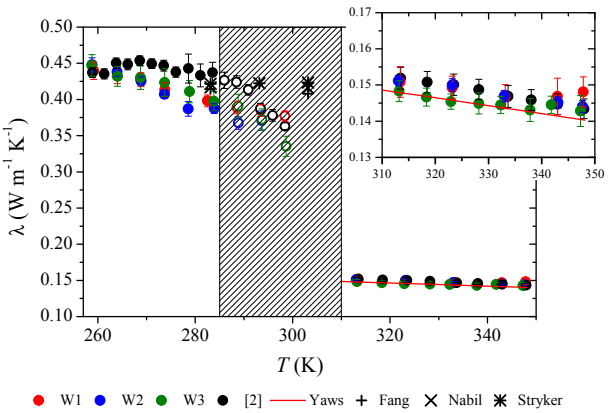

Fig. 7. Thermal conductivity $\lambda(T)$ of n-eicosane as a function of temperature. Data includes measurements in solid state and liquid state. The wires used in each measurement (W1, W2 and W3) are as indicated. The range affected by the heat of fusion is represented as a shadowed region, and the corresponding incorrect data is represented as open symbols. The insert shows a zoom of the data for liquid state. For reference, some literature values are represented: Fang et al. [39], Nabil & Khodadadi [40], and Stryker & Sparrow [41] for solid state; the correlation proposed by Yaws [42] for liquid state; and data by Vélez et al. [2] for both solid and liquid state.

temperature range affected by the heat of fusion effect is highlighted as a shadowed region. It should be noted that full crystallization of *n*-eicosane is a complicated process as it includes an intermediate solid phase (a more detailed discussion in [2]). One consequence is that the temperature range affected by the heat of fusion effect is larger than 7 K, so that the data acquired in solid state at temperatures larger than 285 K is affected, and should be considered as incorrect; this incorrect data is not reported in Table 3.

In agreement with previous results [2] in solid state, the $\lambda(T)$ of *n*-eicosane as shown in Table 3 and Fig. 7 is considered as nearly independent of temperature, or simply, the obtained values do not have enough accuracy to detect a temperature trend. It appears that the values measured with the shorter wires (W1-W3), are slightly lower than the previously published data [2], but consistent with the independent measurements by Fang et al. [39], Nabil & Khodadadi [40], and Stryker & Sparrow [41]. Nevertheless, the detected differences are very small and can be considered insignificant, of course within the intended 7% accuracy. For a clearer understanding of the results in liquid phase, an insert representing a zoom of $\lambda(T)$ in this range is included in Fig. 7. Here, all data sets show a clear decrease of the thermal conductivity with an increase in temperature. The data obtained with the shorter wires are fully consistent, within the experimental uncertainty, with the previously reported values by Vélez et al. [2] as well as with the correlation proposed by Yaws [42].

It can be concluded that the measurement technique and the calibration protocol adopted for short wires is within the experimental accuracy and reproducibility, fully validated by the measurements with *n*-eicosane. Hence, reliable values of $\lambda(T)$, including the phase transition region, can be obtained by the THW method with short wires. This conclusion further assures the reliability of the water *Ih*-ice measurements presented in Section 5.2.

References

[1] M.J. Assael, K.D. Antoniadis, W.A. Wakeham, Historical evolution of the transient hot-wire technique, Int. J. Thermophys. 31 (2010) 1051–1072.
[2] C. Vélez, M. Khayet, J.M. Ortiz de Zárate, Temperature-dependent thermal properties of solid/liquid phase change even-numbered n-alkanes: n-Hexadecane, n-octadecane and n-eicosane, Appl. Energy 143 (2015) 383–394.
[3] C. Vélez, J.M. Ortiz de Zárate, M. Khayet, Thermal properties of n-pentadecane, n-heptadecane and n-nonadecane in the solid/liquid phase change region, Int. J. Therm. Sci. 94 (2015) 139–146.
[4] B. Zalba, J.M. Marin, L.F. Cabeza, H. Mehling, Review on thermal energy storage with phase change: materials, heat transfer analysis and applications, Appl. Therm. Eng. 23 (2003) 251–283.
[5] A. Abhat, Low temperature latent heat thermal energy storage – heat storage materials, Sol. Energy 30 (1983) 313–332.
[6] L.F. Cabeza, A. Castell, C. Barreneche, A. de Gracia, A.I. Fernández, Materials used as PCM in thermal energy storage in buildings: a review, Renew. Sustain. Energy Rev. 15 (2011) 1675–1695.
[7] M.M. Farid, A.M. Khudhair, S.A.K. Razack, S. Al-Hallaj, A review on phase change energy storage: materials and applications, Energy Convers. Manage. 45 (2004) 1597–1615.
[8] S. Himran, A. Suwono, G.A. Mansoori, Characterization of alkanes and paraffin waxes for application as phase change energy storage medium, Energy Sources 16 (1994) 117–128.
[9] K. Kaygusuz, The viability of thermal energy storage, Energy Sources 21 (1999) 745–755.
[10] M. Kenisarin, K. Mahkamov, Solar energy storage using phase change materials☆, Renew. Sustain. Energy Rev. 11 (2007) 1913–1965.
[11] A. Sarı, A. Karaipekli, Thermal conductivity and latent heat thermal energy storage characteristics of paraffin/expanded graphite composite as phase change material, Appl. Therm. Eng. 27 (2007) 1271–1277.
[12] M. Khayet, J.M. Ortiz de Zárate, Application of the multi-current transient hot-wire technique for absolute measurements of the thermal conductivity of glycols, Int. J. Thermophys. 26 (2005) 637–646.
[13] J.R. Vázquez Peñas, J.M. Ortiz de Zárate, M. Khayet, Measurement of the thermal conductivity of nanofluids by the multicurrent hot-wire method, J. Appl. Phys. 104 (2008) 044314.
[14] M.J. Assael, E. Karagiannidis, W.A. Wakeham, Measurements of the thermal conductivity of R11 and R12 in the temperature range 250–340 K at pressures up to 30 MPa, Int. J. Thermophys. 13 (1992) 735–751.
[15] R.A. Perkins, H.M. Roder, C.A. Nieto de Castro, A high-temperature transient hot-wire thermal conductivity apparatus for fluids, J. Res. Natl. Inst. Stand. Technol. 96 (1991) 247–269.
[16] S. Alvarado, E. Marín, Calderon A Juárez, R. Ivanov, A hot-wire method based thermal conductivity measurement apparatus for teaching purposes, Eur. J. Phys. 33 (2012) 897–906.
[17] J.H. Blackwell, Radial-axial heat flow in regions bounded internally by circular cylinders, Can. J. Phys. 31 (1953) 472–479.
[18] J.H. Blackwell, The axial-flow error in the thermal conductivity probe, Can. J. Phys. 34 (1956) 412–417.
[19] H.S. Carslaw, J.C. Jaeger, Conduction of Heat in Solids, Clarendon Press, Oxford, New York, 1959.
[20] M.N. Ozisik, Heat Conduction, John Wiley & Sons, New York, 1993.
[21] C. Vélez, J.M. Ortiz de Zárate, M. Khayet, Thermal conductivity enhancement in nanofluids measured with a hot-wire calorimeter, in: S.M. Musa (Ed.), Nanoscale Flow: Advances, Modeling, and Applications, CRC Press Taylor & Francis Group, 2014.
[22] J.M. Ortiz de Zárate, J.L. Hita, M. Khayet, Legido JL. Measurement of the thermal conductivity of clays used in pelotherapy by the multi-current hot-wire technique, Appl. Clay Sci. 50 (2010) 423–426.
[23] J.J. Healy, J.J.d. Groot, J. Kestin, The theory of the transient hot- wire method for measuring thermal conductivity, Physica 82 (1976) 392–408.
[24] X.-G. Liang, The boundary induced error on the measurement of thermal conductivity by transient hot wire method, Meas. Sci. Technol. 6 (1995) 467–471.
[25] D. Elustondo, M.P. Elustondo, M.J. Urbicain, New thermal conductivity probe design based on the analysis of error sources, J. Food Eng. 48 (2001) 325–333.
[26] M.J. Assael, E. Charitidou, W.A. Wakeham, Absolute measurements of the thermal conductivity of mixtures of alcohols with water, Int. J. Thermophys. 10 (1989) 793–803.
[27] M.L.V. Ramires, C.A. Nieto de Castro, Y. Nagasaka, A. Nagashima, M.J. Assael, W.A. Wakeham, Standard reference data for the thermal conductivity of water, J. Phys. Chem. Ref. Data. 24 (1995) 1377–1381.
[28] Y. Nagasaka, A. Nagashima, Simultaneous measurement of the thermal conductivity and the thermal diffusivity of liquids by the transient hot-wire method, Rev. Sci. Instrum. 52 (1981) 229–232.
[29] S.T. Ro, J.H. Lee, J.Y. Yoo, Onset of Natural Convection Effect in a Transient Hot Wire System, Plenum Press, Thermal Conductivity New York, 1990, pp. 151–164.
[30] X. Zhang, S. Fujiwara, Z. Qi, M. Fujii, Natural convection effect on transient short-hot-wire method, JSMAJ 16 (1999) 129–135.
[31] X. Zhang, M. Fujii, Simultaneous measurements of the thermal conductivity and thermal diffusivity of molten salts with a transient short-hot-wire method, Int. J. Thermophys. 21 (2000) 71–84.
[32] R. Rusconi, W.C. Williams, J. Buongiorno, R. Piazza, L.-W. Hu, Numerical analysis of convective instabilities in a transient short-hot-wire setup for measurement of liquid thermal conductivity, Int. J. Thermophys. 28 (2007) 1131–1146.
[33] A.W. Lawson, R. Lowell, A.L. Jain, Thermal conductivity of water at high pressures, J. Chem. Phys. 30 (1959) 643–647.
[34] R.W. Powell, Thermal conductivities and expansion coefficients of water and ice, Adv. Phys. 7 (1958) 276–297.
[35] E.H. Ratcliffe, The thermal conductivity of ice new data on the temperature coefficient, Phil. Mag. 7 (1962) 1197–1203.

[36] S. Fukusako, Thermophysical properties of ice, snow, and sea ice, Int. J. Thermophys. 11 (1990) 353–372.
[37] O. Andersson, A. Inaba, Thermal conductivity of crystalline and amorphous ices and its implications on amorphization and glassy water, PCCP 7 (2005) 1441–1449.
[38] G.A. Slack, Thermal conductivity of ice, Phys. Rev. B 22 (1980) 3065–3071.
[39] X. Fang, L.-W. Fan, Q. Ding, X. Wang, X.-L. Yao, J.-F. Hou, et al., Increased thermal conductivity of eicosane-based composite phase change materials in the presence of graphene nanoplatelets, Energy Fuels 27 (2013) 4041–4047.
[40] M. Nabil, J.M. Khodadadi, Experimental determination of temperature-dependent thermal conductivity of solid eicosane-based nanostructure-enhanced phase change materials, Int. J. Heat Mass Tran. 67 (2013) 301–310.
[41] P.C. Stryker, E.M. Sparrow, Application of a spherical thermal conductivity cell to solid n-eicosane paraffin, Int. J. Heat Mass Tran. 3 (1990) 1781–1793.
[42] C.L. Yaws, Handbook of Thermodynamic and Physical Properties of Chemical Compounds, N.Y. Knovel, Norwich, 2003.